Analytical design and modelling of power converters equipped with synthetic inertia control.

Alberto Bolzoni, Cristina Terlizzi, Roberto Perini
POLITECNICO DI MILANO
via La Masa 34,
20156 Milano, Italy
Tel.: +39 02 2399 8523
E-Mail: alberto.bolzoni@polimi.it, roberto.perini@polimi.it

Keywords

«Microgrids», «Control methods for electrical systems», «Converter control», «Renewable energy systems», «Distributed power»

Abstract

This paper deals with a design strategy for the provision of fast-response synthetic inertia services from a grid-connected converter interfaced to the low-voltage grid by means of a constant power control structure, like the one traditionally implemented for renewables generators. The novelty introduced lies in the inclusion of the external grid characteristics in the definition of the current-controlled inertia loop; this analytical approach allows to predict the stability of the dynamics associated to the grid itself and to the converter during inertia provision.

Introduction

The integration of PQ-controlled generators in power systems is becoming a serious problem both as regards transmission networks as well as for low-voltage microgrids: the increase of renewables is causing a higher percentage of production to be interfaced to the grids by means of a regulation scheme that does not allow a direct feedback between the injected power and the actual balancing state of the system.
According to European ENTSO-E directives [1], the provision of inertia services to the grid is becoming a factual problem [2]; at a national level, the Italian grid code has recently introduced new technical constraints for photovoltaic units connected to medium and high voltage public grids during over-frequency transients: the converter should curtail active power at the interface according to a negative-slope linear behaviour with respect to system frequency as soon as the higher limit of the dead-band is reached; this can be obtained by acting on the MPPT control of the PV generator. The intrinsic drawback of this approach lies in the fact that currently no constraints are prescribed when the network is undergoing an under-frequency condition. A possible solution consists in keeping a margin with respect to the Maximum Power Point Tracking (MPPT) conditions, to use such a reserve for grid sustainment in case of under-frequency [3]-[4]; however, this technique implies the knowledge of the maximum available power even in de-loading conditions to guarantee the regulation service when required [5]-[6].
Another possible solution consists in generating a transitory power response during frequency transients: this property goes under the name of synthetic inertia and it is defined as the capability of a PQ-controlled converter to modulate its injected power when an external unbalance between load and generation is causing a frequency drift on the network. In this way it is emulated the presence of a rotating machine by means of electronic converters. For photovoltaic plants, a storage unit or a super-capacitor has to be placed in parallel to the DC bus to be able to provide the required regulating energy.
Consistent work has been done on numerical simulations related to the synthetic inertia implementation at a system level, considering both wind generators [7]-[8], storage and supercapacitor units [9]. Still it seems that a clear proposal for an analytical design of the control parameters that includes both the characteristics of the grid and the stability margins of the converter during regulation service is currently unavailable: this paper tries to focus the attention on such a perspective.

System model

External grid model

Consider the model of a three-phase grid-connected converter, interfaced to an external grid by means of a LC filter and a transformer (Figure 1.a); the grid is represented by an inductive-resistive impedance (R_g, L_g) in series with a sinusoidal voltage source ($\bar{v}_g$).

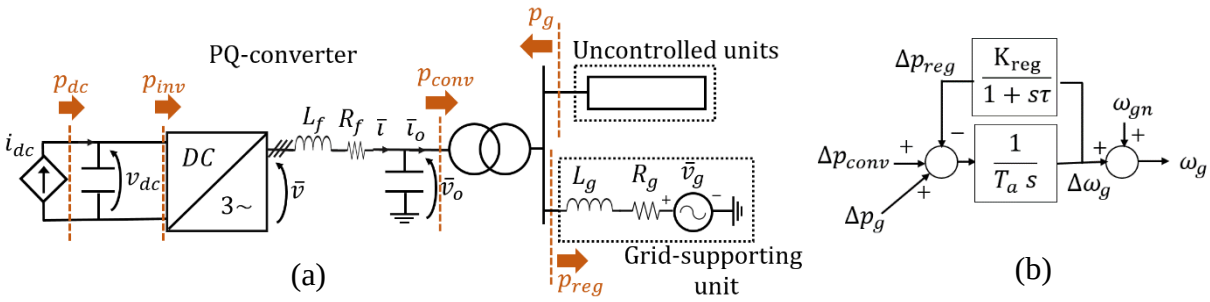

Fig. 1: (a) Equivalent structure of the system and (b) linearized model of the grid used for frequency transients' analysis. In the system structure is shown the convention adopted for power measurement.

The fundamental frequency of the grid takes into account the primary regulation performed by the grid-forming units and the inherent inertia of the system. Typically, the PQ converter acts as a constant power source, thus $\Delta p_{conv} = 0$; under these conditions the primary frequency regulation can be modelled according to (1) and (2),

$$\omega_g = \omega_{gn} + K_g(s) \cdot \Delta p_g \quad (1)$$

$$K_g(s) = \frac{\Delta\omega_g}{\Delta p_g} = \frac{(1+s\tau)}{s^2 T_a \tau + s\, T_a + K_{reg}} \quad (2)$$

where T_a is the equivalent inherent starting time of the inertia frequency regulation, τ is the delay associated to the primary regulation, K_{reg} is the regulating energy and Δp_g is the power imbalance on the grid, given by the difference between generation change and load change $\Delta p_g = \Delta p_{gen} - \Delta p_{load}$. On the other hand, when synthetic inertia is introduced, the contribution Δp_{conv} of the PQ-converter during frequency transients is not null; thus, in the following, it will be developed a model whose aim is to underline the dynamics of the frequency transients during synthetic inertia provision.
It is worth noting that all the values are referred to the per unit reference system of the converter, while in general the characteristics of the external grid are referred in respect to its nominal regulating power; thus the following base-transformation has to be performed: $T_a = T_a' \cdot A_b' / A_b$, $K_{reg} = K_{reg}' \cdot A_b' / A_b$ and $\Delta p_g = \Delta p_g' \cdot A_b' / A_b$, being A_b the base power of the PQ converter and A_b' the one of the grid. This allows to take into account the mutual strength in terms of regulating power between the PQ converter and the external grid which is performing primary regulation (the external grid may be either another converter with droop control or a traditional generator).
In this perspective, the proposed design model adapts both to the case of a strong power system or a weak droop-controlled microgrid in island mode, provided that the correct numerical values are used; in the following, it will be shown the formal equivalence in the two cases. In case of a portion of MV/HV grid is deliberately or unintentionally operated in island conditions, the converter represents the aggregate of all the renewable generators controlled with a PQ scheme.

Non-linear system model

Figure 2 shows the general structure of the control system: as in a traditional PQ scheme [10], an external DC-bus control with a slow pass-band defines the reference for the internal active power control; as for the reactive contribution, it is assumed an external constant reference Q_{ref}.

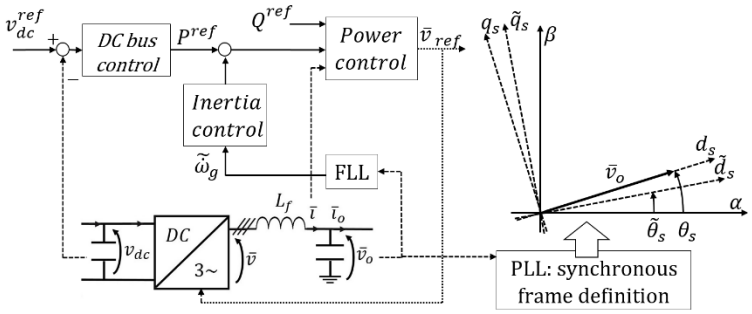

Fig. 2: Structure of the control system. It consists of an external DC-bus voltage control and an internal power control; a frequency-locked loop (FLL) estimates the derivative of the angular frequency $\tilde{\omega}_g$. An independent phase-locked loop (PLL) determines the estimated synchronous control frame $\tilde{d}\tilde{q}_s$ with respect to the real one dq_s.

Considering the physical system (Figure 2), it is possible to derive the equation associated to the inductive filter, referred to the rotating frame dq_s aligned with the capacitor voltage $\bar{v}_o$, whose angle is θ_s. All the quantities are expressed in per unit as space vectors in the Park domain ($p = \frac{d}{dt}$):

$$\bar{v} = \bar{v}_o + j\omega_s L_f \bar{\imath} + L_f \frac{p}{\omega_b} \bar{\imath} + R_f \bar{\imath} \tag{3}$$

In the equation above, ω_s represents the per-unit time-derivative of the angle θ_s: $\omega_s = p\theta_s/\omega_b$.
To align the control system to the synchronous frame, the estimation $\tilde{\theta}_s$ of the voltage angle is carried out by means of a phase-locked loop (PLL) algorithm generally used for the synchronization of PQ-controlled units [10]. This generates the frame of the control system indicated as $\tilde{d}\tilde{q}_s$ (Figure 2): the angular difference $(\theta_s - \tilde{\theta}_s)$ represents the error of the PLL.
The dynamic of the DC-bus can be obtained from the capacitor power balance:

$$p\left(\frac{1}{2} C_{dc} \cdot (V_{b\,dc} \cdot v_{dc})^2\right) = (p_{dc} \cdot A_b - p_{inv} \cdot A_b) \tag{4}$$

$$C_{dc} \cdot v_{dc} \cdot p\, v_{dc} \cdot (V_{b\,dc}^2 / A_b) = (p_{dc} - p_{inv}) \tag{5}$$

where C_{dc} is the capacitance of the DC-bus, A_b and $V_{b\,dc}$ are the values of base power and DC voltage, v_{dc} is the per-unit DC voltage and $(p_{dc} - p_{inv})$ represents the charging power of the capacitor in per unit. Defining $\tau_{dc} = C_{dc} \cdot V_{b\,dc}^2 / A_b$ and assuming a lossless behaviour of the inverter, the following non-linear equation can be derived:

$$\tau_{dc} v_{dc} \cdot p\, v_{dc} = p_{dc} - p_{inv} \cong p_{dc} - \ Re\{\bar{v}_{dq_s} \bar{\imath}_{dq_s}^*\} \tag{6}$$

As for the inertia control, it behaves as an additional active power reference proportional to the frequency approximate derivative $\tilde{\omega}_g$; in order to extract the signal derivative avoiding the disturbances generated by numeric derivation, a QSOGI-FLL algorithm [11] has been introduced. It has been chosen to keep separate the derivative estimation from the synchronous-frame definition to increase the degrees of freedom associated to the design of the control system. According to [11], the linearization of the FLL block leads to the following approximation between the estimated derivative $\tilde{\omega}_g$ and the real angular frequency ω_g, where ω_{FLL} is the cut-off frequency of the QSOGI-FLL loop:

$$\tilde{\omega}_g = \frac{s}{1 + s/\omega_{FLL}}\, \omega_g \tag{7}$$

The complete non-linear model associated to the dynamics of the system is reported in Figure 3 for completeness. All the quantities of the physical system are referred to the frame dq_s, while the variables of the control are synchronous with the estimated one $\tilde{d}\tilde{q}_s$.

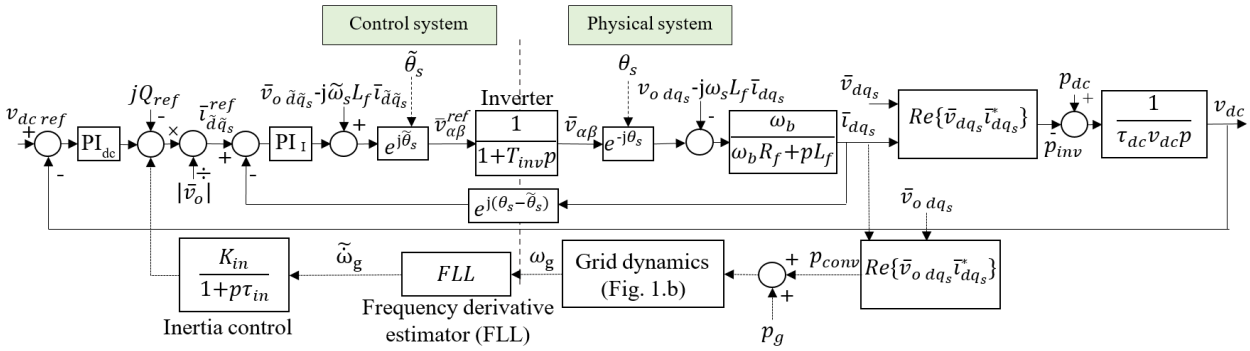

Fig. 3: Complete non-linear model of the system, which includes PQ-converter and grid dynamics.

Linearized model

Starting from the complete system (Figure 3), the linearized models for active and reactive power control, corresponding to direct and quadrature axis components, are shown in Figure 4. The following approximations are introduced during the derivation of the linearized system:

- given its high pass-band, the effect associated to the PLL is negligible; thus $\theta_s - \tilde{\theta}_s \cong 0$ and a single frame dq can be considered, with angular frequency ω_s;
- assuming a small voltage drop on the filter, the magnitude of the Park voltage $\bar{v}_o$ is close to $\bar{v}$: $|\bar{V}_o| = |V| \cong V_d$ and $v_{oq} = v_q = 0$;
- low power losses on the interface filter: $p_{inv} = Re\{\bar{v}_{dq_s}\bar{\imath}^*_{dq_s}\} \cong p_{conv} = Re\{\bar{v}_{o\,dq_s}\bar{\imath}^*_{dq_s}\}$

The DC-bus linearized dynamic is calculated as:

$$\tau_{dc}(V_{dc}+\Delta v_{dc})\cdot p(V_{dc}+\Delta v_{dc}) = (V_{dc}+\Delta v_{dc})\cdot(I_{dc}+\Delta i_{dc}) - (V_d+\Delta v_d)\cdot(I_d+\Delta i_d) \quad (8)$$

By neglecting second order differentials and considering the derivative of the steady-state solution equal to zero, it is possible to derive:

$$\tau_{dc}V_{dc}p\Delta v_{dc} = V_{dc}I_{dc} + V_{dc}\Delta i_{dc} + I_{dc}\Delta v_{dc} - (V_d I_d + V_d\Delta i_d + I_d\Delta v_d) \quad (9)$$

Now considering that $V_{dc}I_{dc} = V_d I_d$ at steady state and assuming a negligible value of the voltage increase Δv_d, the final linear equation is retrieved and transformed to the Laplace domain:

$$\Delta v_{dc} = \frac{V_d}{(I_{dc}-\tau_{dc}V_{dc}s)}\Delta i_d - \frac{V_{dc}}{(I_{dc}-\tau_{dc}V_{dc}s)}\Delta i_{dc} \quad (10)$$

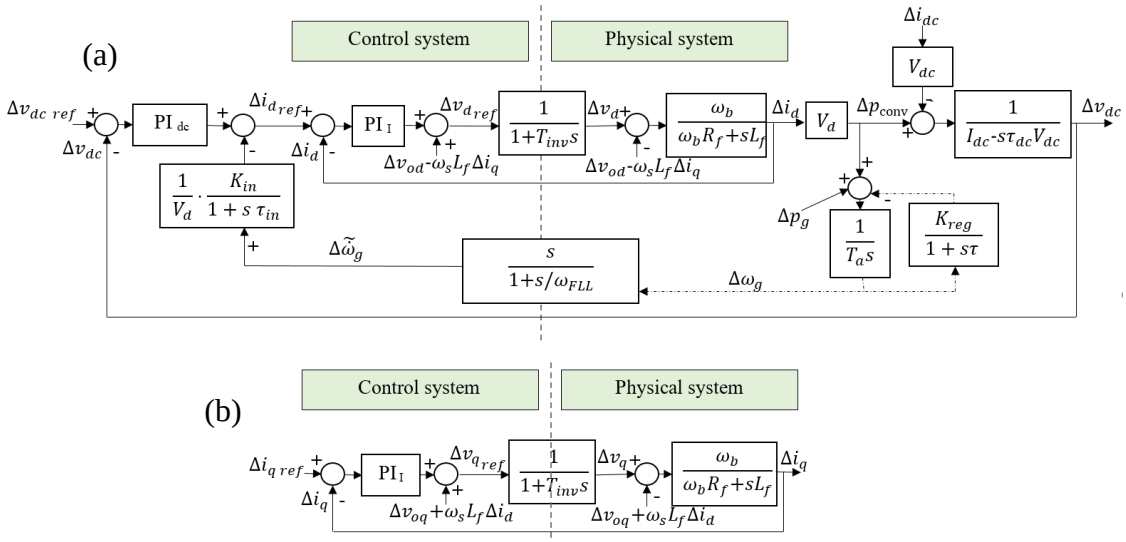

Fig. 4: Linearized model for the design of the control system – direct (a) and quadrature (b) axis.

The design of the selective inertia is performed including the external grid model into the linearized system. The linearized model allows to derive the equivalent open-loop function associated to the inertia control (Figure 5), which is given by:

$$L(s) = \frac{s}{1+s/\omega_{FLL}} \cdot \frac{K_{in}}{1+s\tau_{in}} \cdot K_g(s) \cdot KI(s) \tag{11}$$

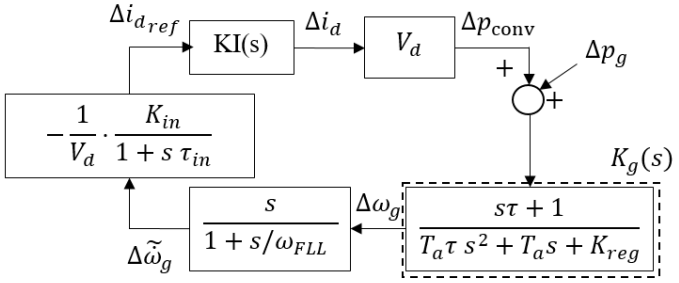

Fig. 5: Equivalent control loop associated to the inertia regulation.

Inertia provision in droop-controlled microgrids

Equivalence between primary regulation and droop models

In this section it will be analysed the case of inertia provision for a low-voltage microgrid where primary regulation is carried out by means of droop control (grid supporting element in Figure 1). To exploit the above-mentioned model, a formal equivalence between droop and primary frequency regulation is carried out: in this way it will be analysed the equivalent inertia provided by the droop-controlled converters in island microgrids. Here it is considered the transfer function of the droop as generally presented in literature [12] - [13], including linear m coefficient, equivalent delay introduced by the internal voltage control of the converter τ_{droop} and time constant used for active power calculation T_p:

$$K_{droop}(s) = \frac{\Delta\omega_g}{\Delta p_g} = \frac{1}{(1+\,s\cdot\tau_{droop})} \cdot \frac{m}{1+s\cdot T_p} \tag{12}$$

Droop transfer function (12) is formally equal to the one used for traditional grids (2). It is possible to retrieve the coefficients equivalence by pole comparison of (12) and (2), considering the small value of τ_{droop} (in particular $\tau_{droop} \ll T_p$):

$$\tau = \tau_{droop} \qquad \mathrm{T_a} = \frac{T_p}{m} \qquad K_{reg} = \frac{1}{m} \tag{13}$$

The important result associated to the proposed method lies in the parallelism that can be obtained between high-inertia traditional systems and low-inertia microgrids; this enables the adoption of the proposed design model for selective inertia provision for both cases, simply changing the numerical values of the actual study case of interest.

Inertia design for droop-controlled microgrids

Consider the case of a droop-controlled microgrid; given the typical values of the droop parameters reported in literature [12] - [13], it is very common that a pole of the grid transfer function $K_g(s)$ (2) simplifies with the zero, thanks to the small value of the equivalent delay τ associated to the droop. Thus, in this case the equivalent transfer function of the grid can be approximated as a first order system:

$$K_g\,(s)\big|_{\tau\to 0} \cong \frac{1}{T_a s+K_{reg}} \tag{14}$$

Neglecting the effect of the internal current control generally much faster than the considered dynamics ($KI(s) \cong 1$), the open loop function associated to the inertia control becomes (Figure 5):

$$L(s) \cong \frac{s}{1+s/\omega_{FLL}} \cdot \frac{K_{in}}{1+s\tau_{in}} \cdot \frac{1}{T_a s+K_{reg}} \tag{15}$$

which, for $\omega < 1/\tau_{in}$, gives an approximate closed loop function (Figure 5) equal to:

$$K'_g(s) = \frac{\Delta\omega_g}{\Delta p_g} = \frac{K_g(s)}{1+L(s)} \cong \frac{1}{(T_a+K_{in})\cdot s+K_{reg}} \tag{16}$$

The introduction of the selective inertia moves the pole of the grid to lower frequencies, contributing to the slow-down of the frequency transients; the equivalent starting time becomes:

$$T_a^{eq} = T_a + K_{in} \quad \text{for } \omega < 1/\tau_{in} \tag{17}$$

A sufficient condition for the stability of the inertia loop is given by $\frac{K_{in}}{T_a} < 1$, as $|L(j\omega)| < 1 \; \forall \; \omega$.

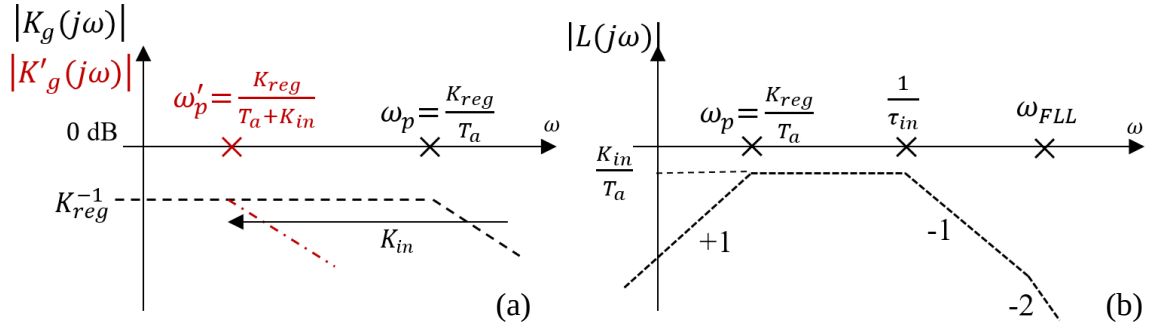

Fig. 6: (a) Bode diagram of the equivalent grid transfer function, with and without synthetic inertia provision in the case of microgrids. The introduction of the selective inertia moves the cut-off frequency of the grid function towards lower values. (b) Simplified open-loop function associated to the inertia control.

Additionally, as the pole of the inertia regulator is moved to higher frequencies, the lower is the stability margin associated to the inertia loop. For $1/\tau_{in} \cong \omega_{FLL}$ the sufficient condition becomes necessary as the crossing of the 0 dB axes occurs with slope -2: the system becomes unstable for the Bode criterion.

Case study and results

The proposed method has been validated considering the values associated to a PQ converter operated in parallel to a droop-controlled unit in island mode (grid supporting element in Figure 1). The two converters are characterized by the same nominal power; parameters used for the simulation are shown in Table I and Table II for the two converters respectively.

Table I: System parameters for PQ converter

Parameter	Numeric value
Base power A_b, Base angular frequency ω_b	2.4 kVA, $2\pi \cdot 50$ rad/s
Base voltages: V_b (AC), $V_{b\,dc}$ (DC)	200 V rms, $\sqrt{2}\cdot 200$ V
Current ω_{cI} and voltage ω_{cV} loops cut-off frequencies	$2\pi \cdot 350$ rad/s, $2\pi \cdot 1$ rad/s
Filter parameters R_f, L_f	0.0072 p.u. , 0.0448 p.u.
FLL cut-off frequency ω_{FLL}	100 rad/s
Inertia control time constant τ_{in}	60 rad/s

Table II: Equivalent characteristic of the droop unit

Parameter	Numeric value
Droop coefficient m	0.02 p.u.
Droop time constant T_p	0.2 s
Equivalent delay τ_{droop}	$(2\pi \cdot 50)^{-1}$ = 3.2 ms

By recalling the formal correspondence between primary regulation and droop (13), it is possible to derive the equivalent grid parameters associated to this study case: $\tau = 3.2$ ms, $T_a = 10\ s$, $K_{reg} = 50$ p.u. associated to the model in (2). Poles and zeros can be approximated (for $\tau \to 0$) considering the linearized behaviour of the square root:

$$p_{1,2} = -\frac{1}{2\tau} \cdot \left(-1 \pm \sqrt{1 - \frac{4\tau K_{reg}}{T_a}}\right) \cong \begin{cases} p_1 \cong -K_{reg}/T_a \\ p_2 \cong -1/\tau \end{cases} \quad (18)$$

Leading to the cancellation of pole p_2 with the corresponding zero $z_1 = -1/\tau$.
In this case the exact values are: $p_1 = -5$ rad/s, $p_2 = -309$ rad/s, $z_1 = -314$ rad/s).

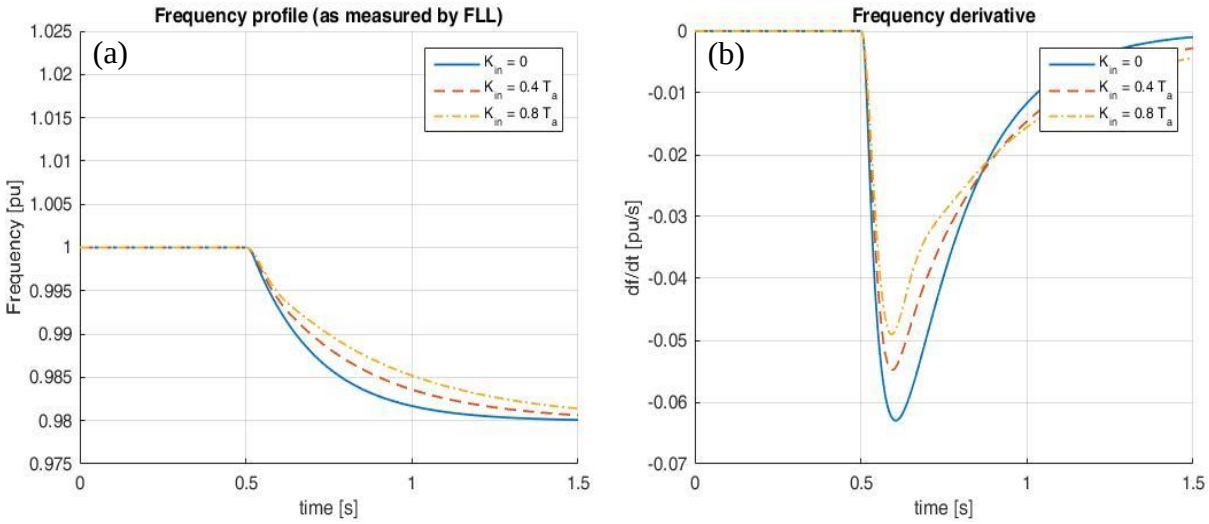

Fig. 7: (a) Frequency transient profile and (b) estimated FLL derivative with different inertia provision in the case of droop-controlled microgrids.

The derived stability condition is verified considering $K_{in} = 1.2\ T_a$: according to the mathematical model the system should tend to instability. This is confirmed by the simulation: oscillations occur as soon as the inertia loop is inserted (Figure 8).

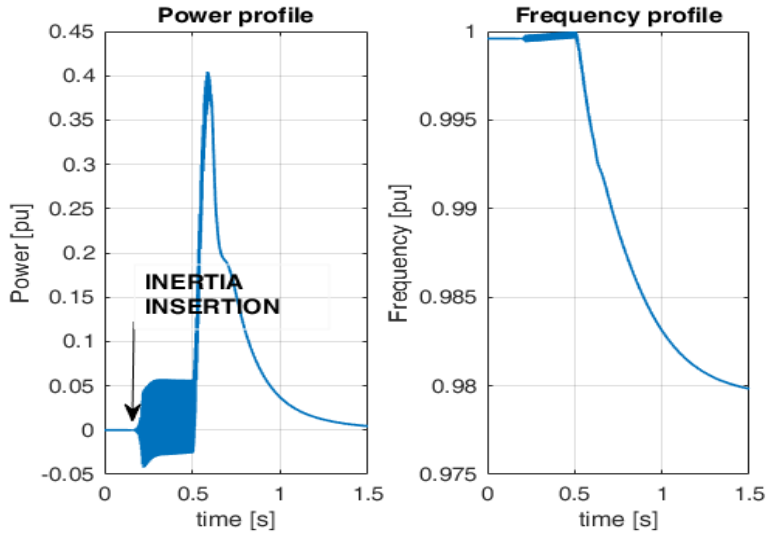

Fig. 8: Unstable behaviour for $K_{in} = 1.2\ T_a$; this result confirms the mathematical correctness of the derived model.

Inertia provision in traditional grids

Inertia design for traditional grids

Synthetic inertia becomes especially useful in case primary regulation is performed by traditional machines with longer response delays during power transients. Differently from the case of droop where the time delay τ is negligible, for traditional grids the provision of primary regulation service occurs with an internal delay comparable with the grid starting time T_a. Under these conditions, the analysis of the equivalent grid transfer function $K_g(s)$ in Figure 9 shows the presence of a couple of complex conjugate poles with natural frequency $\omega_n = \sqrt{\mathrm{K_{reg}}/(T_a\tau)}$ and damping $\xi = 0.5\sqrt{\mathrm{T_a}/(\tau\, K_{reg})}$. In the common case where $\xi < \sqrt{2}/2$, this gives rise to a resonance peak in $\omega_p \cong \omega_n$ that produces oscillatory behaviours in the frequency time-response. The introduction of the selective inertia changes the properties of the equivalent grid transfer function according to the procedure already shown in the case of a microgrid:

$$K'_g(s) = \frac{K_g(s)}{1+L(s)} \cong \frac{(1+s\tau)}{s^2(T_a\tau+K_{in}\tau)+s\,(T_a+K_{in})+K_{reg}} \quad \text{for} \quad \omega < 1/\tau_{in} \tag{19}$$

that corresponds to an equivalent natural frequency of $\omega'_n = \sqrt{K_{reg}/(T_a\tau + K_{in}\tau)}$ and a damping of $\xi' = 0.5\sqrt{(\mathrm{T_a} + K_{in})/(\tau\, K_{reg})}$. The introduction of the inertia provision reduces the equivalent natural frequency of the grid and increases the equivalent damping; the magnitude of the resonance peak reduces according to the diagram shown in Figure 9.

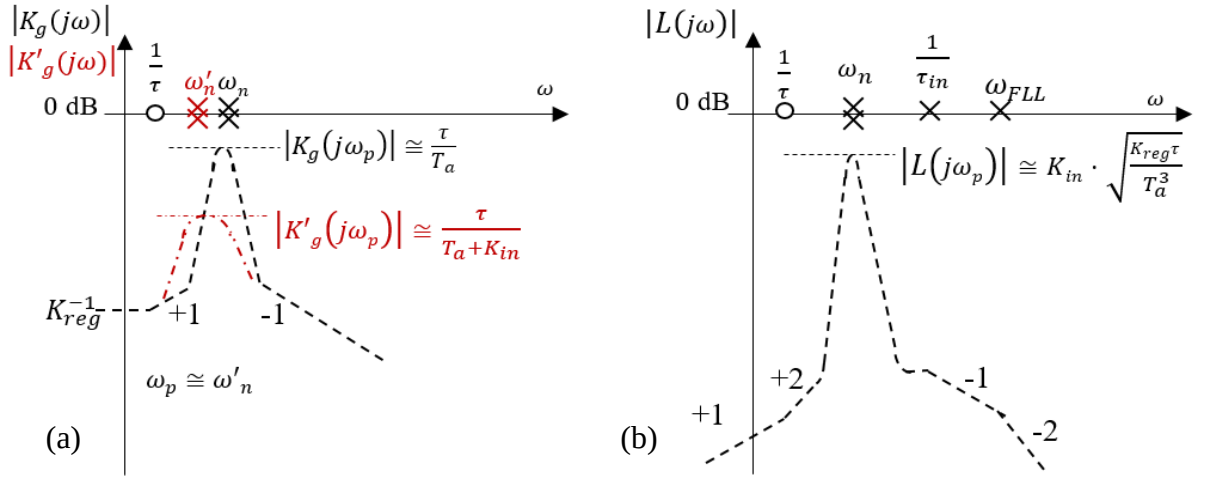

Fig. 9: (a) Equivalent grid function without synthetic inertia (dashed line) and with synthetic inertia (dashed-dotted line); (b) open-loop transfer function of the selective inertia loop. All the quantities reported in the graph are analytically derived from the corresponding transfer functions.

A sufficient condition for stability is $|L(j\omega_p)| < 1$ thus:

$$\frac{K_{in}}{T_a} < \sqrt{\frac{T_a}{K_{reg}\tau}} \tag{20}$$

Case study and results

The proof of the proposed approach has been verified by means of simulations, introducing the actual discretization both in the converter control and in the measurement of frequency derivative with the QSOGI-FLL algorithm. For equal comparison, it has been chosen a study case in which the regulating energy K_{reg} and starting time T_a are the same as the ones considered in the microgrid case; on the other hand, the delay τ has been increased up to the values generally obtainable with the traditional primary regulation. Parameters used for the simulation are recalled in Table III while results are in Figure 10.

Table III: System parameters for slow-regulation grids

Parameter	Numeric value
Regulating energy K_{reg}	50 p.u.
Starting time T_a	10 s
Equivalent delay τ	0.5 s

In the simulation, a load step-change with $\Delta p_g = -1$ p.u. has been introduced at $t = 0.5\ s$; results associated to the frequency value and to the measured derivative are reported below.

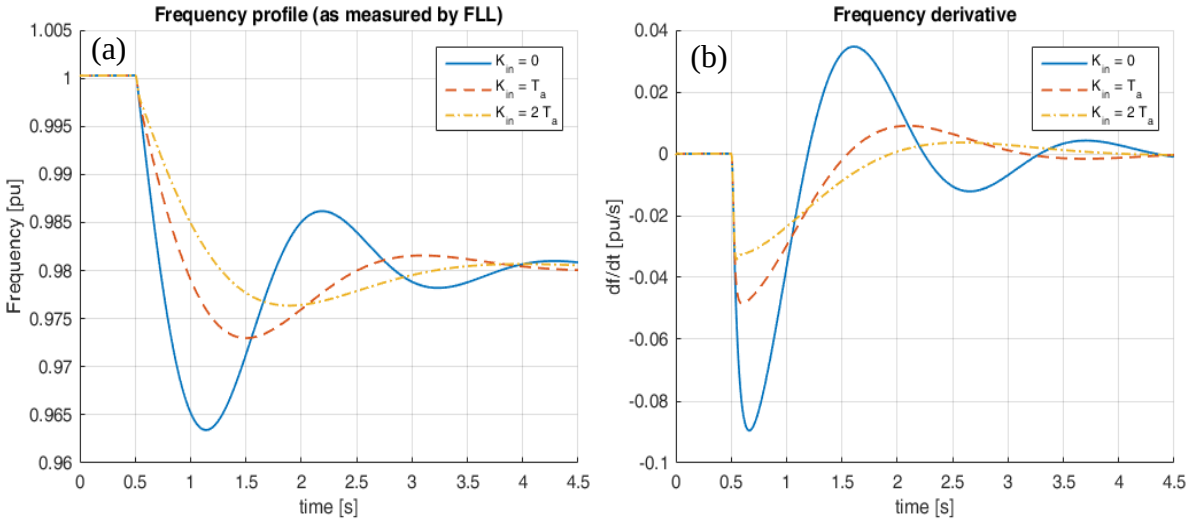

Fig. 10: (a) Frequency and (b) measured derivative with inertia provision in the case of traditional grids.

To assess the correctness of the derived mathematical model, transient characteristics derived from simulated behaviour are compared to the theoretical ones associated to the model (Table IV). Tables shows that the predicted dynamic properties are obtained also in the simulation: the correspondence confirms the correctness of the mathematical derivation. Moreover, it is possible to see that the inertia-less case is characterized by a higher uncertainty due to the cancellation of higher-order dynamics.

Table IV: Comparison between theoretical and simulated results

Transient characteristic	Case	Expected value	Simulated result
Steady state value $\omega^* = \omega_o + \Delta P_g / K_{reg}$ $(\Delta P_g = 1\ p.u.)$	$K_{in} = 0, T_a, 2T_a$	0.98 p.u.	0.98 p.u.
Natural frequency $\omega_n' = \sqrt{K_{reg}/(T_a\tau + K_{in}\tau)}$	$K_{in} = 0$	3.16 rad/s	-
	$K_{in} = T_a$	2.23 rad/s	-
	$K_{in} = 2 \cdot T_a$	1.82 rad/s	-
Damping factor $\xi' = 0.5\sqrt{(T_a + K_{in})/(\tau\, K_{reg})}$	$K_{in} = 0$	0.31	-
	$K_{in} = T_a$	0.44	-
	$K_{in} = 2 \cdot T_a$	0.54	-
Period of the oscillation $T = 2\pi / \left(\omega_n' \cdot \sqrt{1 - \xi'^2}\right)$	$K_{in} = 0$	2.09 s	2.13 s
	$K_{in} = T_a$	3.14 s	3.07 s
	$K_{in} = 2 \cdot T_a$	4.12 s	4.21 s
Overshoot $\frac{(\omega_{min} - \omega^*)}{\omega^*} = \exp\left(-\xi'\pi / \sqrt{1 - \xi'^2}\right)$	$K_{in} = 0$	40 %	70 %
	$K_{in} = T_a$	22 %	35 %
	$K_{in} = 2 \cdot T_a$	14 %	18 %

Conclusion

In this paper are analysed the effects associated to the introduction of a synthetic inertia loop in the control of a power converter. Starting from the traditional PQ scheme generally adopted for renewables or storage applications, an additional current feedback with an approximated derivative controller has been considered.
Starting from the non-linear model of the control, the simplified linearized system has been derived with the objective of inertia parameters tuning; the proposed method has been validated considering both the case of a droop-controlled microgrid and the one of a power network with traditional primary regulation. The analysis confirms the strong effect of the control parameters on the system stability and the mathematical validity of the proposed model. In this perspective, it becomes evident the need to estimate in real-time the equivalent system inertial properties to introduce an automatic tuning of the parameters associated to the control. This aspect could be developed in future works.

References

[1] ENTSO-E, “Need for synthetic inertia (SI) for frequency regulation - ENTSO-E guidance document for national implementation for network codes on grid connection”. Available at: https://www.entsoe.eu

[2] Terna, Italian Grid Code, Allegato A70, “Regolazione tecnica dei requisiti di sistema della generazione distribuita”, pp. 6. Available at: http://www.terna.it/en-gb/sistemaelettrico/codicedirete.aspx

[3] P.P. Zarina, S. Mishra, P.C. Sekhar, Exploring frequency control capability of a PV system in a hybrid PV-rotating machine-without storage system, In International Journal of Electrical Power & Energy Systems, Volume 60, 2014, Pages 258-267

[4] Sotirios I. Nanou, Apostolos G. Papakonstantinou, Stavros A. Papathanassiou, A generic model of two-stage grid-connected PV systems with primary frequency response and inertia emulation, In Electric Power Systems Research, Volume 127, 2015, Pages 186-196

[5] A. Hoke, E. Muljadi and D. Maksimovic, "Real-time photovoltaic plant maximum power point estimation for use in grid frequency stabilization," 2015 IEEE 16th Workshop on Control and Modeling for Power Electronics (COMPEL), Vancouver, BC, 2015, pp. 1-7.

[6] E. I. Batzelis, G. E. Kampitsis and S. A. Papathanassiou, "Power Reserves Control for PV systems With Real-Time MPP Estimation via Curve Fitting," in IEEE Transactions on Sustainable Energy, vol. 8, no. 3, pp. 1269-1280, July 2017.

[7] J. Van de Vyver, J. D. M. De Kooning, B. Meersman, L. Vandevelde and T. L. Vandoorn, "Droop Control as an Alternative Inertial Response Strategy for the Synthetic Inertia on Wind Turbines," in IEEE Transactions on Power Systems, vol. 31, no. 2, pp. 1129-1138, March 2016.

[8] W. He, X. Yuan and J. Hu, "Inertia Provision and Estimation of PLL-Based DFIG Wind Turbines," in IEEE Transactions on Power Systems, vol. 32, no. 1, pp. 510-521, Jan. 2017.

[9] M. F. M. Arani and E. F. El-Saadany, "Implementing Virtual Inertia in DFIG-Based Wind Power Generation," in IEEE Transactions on Power Systems, vol. 28, no. 2, pp. 1373-1384, May 2013.

[10] J. Rocabert, A. Luna, F. Blaabjerg; P. Rodríguez, “Control of Power Converters in AC Microgrids” IEEE Trans. on Power Electronics, Vol 27, Issue 11, 2012, pp. 4734 – 4749.

[11] R. Teodorescu, M. Liserre, P. Rodriguez, "Grid Synchronization in Three-Phase Power Converters," in Grid Converters for Photovoltaic and Wind Power Systems, 1, Wiley-IEEE Press, 2011, pp.416.

[12] Y. Sun, X. Hou, J. Yang, H. Han, M. Su and J. M. Guerrero, "New Perspectives on Droop Control in AC Microgrid," in IEEE Transactions on Industrial Electronics, vol. 64, no. 7, pp. 5741-5745, July 2017.

[13] A. Bolzoni, G. M. Foglia, L. Frosio, M. F. Iacchetti and R. Perini, "Impact of line and control parameters on Droop Stability in Inverters for Distributed Generation," in IEEE Transactions on Smart Grid, doi 10.1109/TSG.2017.2717869